Microgravity Science and Technology (2022) 34: 61
https://doi.org/10.1007/s12217-022-09989-6

ORIGINAL ARTICLE

The Micro-Deformation Monitoring Based on the All-Fiber-Optic Sensor in Taiji Program

Juan Wang[1,2,3] · Heshan Liu[1,2] · Ya Zhao[4] · Ruihong Gao[5] · Ran Yang[1] · Ziren Luo[1,2]

Received: 1 December 2021 / Accepted: 8 July 2022 / Published online: 16 July 2022

Abstract

To reach the requirement of the high precision displacement measurement in Taiji program, it is necessary to reject the optical path noises caused by the structure deformation. Different from the spatial optical path establishment, we present a methodology to monitor the micro-deformation based on the all-fiber-optic sensor, which can be pasted to the surface of the target components. In this paper, the all-fiber-optic sensor is applied to reflect the deformation of the cantilever beam as an example. The experimental results reveal that the sensing scheme adequately aligns with the theoretical predictions with the acceptable tolerance for error, and the deformation measurement error of the sensor is reduced from 240 nm to 17.2 nm through the noise suppression scheme. It validates the feasibility of the contact and the high precision micro-deformation measurement and turns out to be a promising candidate to monitor the surface micro-deformation of the target components, such as the optical platform, the telescope framework and the satellite structure in the future Taiji program.

Keywords Taiji program · Micro-deformation · All-fiber-optic sensor · Contact and high precision measurement

Introduction

The Taiji program is proposed for the gravitational waves (GWs) detection with frequencies covering the range of 0.1 mHz to 1.0 Hz Hu and Wu (2017); Hu and Kang (2020); Luo (2018). It requires the displacement measurement precision to reach 1 pm/$\sqrt{Hz}$ in the related frequency range by the laser interferometer Liu and Luo (2021). It is essential to consider the influence of the structure micro-deformation, caused by the force, vibration or temperature. For example, the extra aberration can be produced when the telescope framework is deformed axially or laterally; the deformation of the interference platform will result in the optical path noises. Generally, two noise suppression methods are provided to achieve the precision requirement. One scheme is to reduce the deformation directly by stabilizing the environment, which can be realized by building the vibration or thermal isolation system Tröbs et al. (2013). The other one is to find the relationship between the noise sources and the

TC: Pioneer WR Hu - Research Pioneer and Leader of Microgravity Science in China: Dedicated to the 85th Birthday of Academician Wen-Rui Hu
Guest Editors: Jian-Fu Zhao, Kai Li

✉ Ziren Luo
luoziren@imech.ac.cn

Juan Wang
wangjuan@imech.ac.cn

Heshan Liu
liuheshan@imech.ac.cn

Ya Zhao
zhaoya16@mails.ucas.edu.cn

Ruihong Gao
gaoruihong@imech.ac.cn

Ran Yang
yangran@imech.ac.cn

[1] Center for Gravitational Wave Experiment, National Microgravity Laboratory, Institute of Mechanics, Chinese Academy of Sciences, Beijing 100190, China

[2] Taiji Laboratory for Gravitational Wave Universe (Beijing/Hangzhou), University of Chinese Academy of Sciences, Beijing 100049, China

[3] School of Engineering Science, University of Chinese Academy of Sciences, Beijing 100049, China

[4] Changchun Institute of Optics, Fine Mechanics and Physics, Chinese Academy of Sciences, Changchun 130033, China

[5] School of Fundamental Physics and Mathematical Sciences, Hangzhou Institute for Advanced Study, UCAS, Hangzhou 310024, China

interference results, followed by the noises' effect subtraction from the final interference data. The former is limited in some cases where the noises can't be rejected totally. The latter is more convincing and it needs the real-time environmental monitoring of the deformation of the target surface. It can be obtained by the laser interference ranging, in which many reflective glasses are placed in the assigned surface. However, it requires the demanding accuracy of the optical path assembly and adjustment. Most importantly, it may bring the stray light to the scientific interferometer. Hence, during the operation, it is necessary to design a contact sensor to measure the real-time micro-deformation on the surface of the related components.

The fiber optic interferometric sensor has been selected for various benefits of high sensitivity, small size, geometric flexibility and immunity from the electromagnetic interference Sun et al. (2021). It has been widely used in environmental measurements, such as deformation, micro-vibration, strain, temperature, humidity, pressure and other parameters Wang et al. (1996); Sun et al. (2007); BoIler et al. (2009). To be consistent with the interferometer configuration in Taiji program, Michelson interferometer is selected to perform a contact and high precision sensor sensitive to the structure deformation in our research. The standard fiber optic strain gauge has been depicted in a form of Michelson interferometer in terms of the optical phase difference (OPD) between the sensitive and the reference optical paths Malki et al. (1995); Butter and Hocker (1978). It utilized the motion of interference fringes to measure the strain in cantilever beam through the fiber optic cemented into it. After that, most researches have been focused on increasing the measurement accuracy and broadening the application of the Michelson optical fiber interferometric sensor. For instance, a practical coupling device based on a two-core fiber can be used as an anisotropic coupler Vallée and Drolet (1994). The in-fiber integrated Michelson interferometer has been investigated by designing and fabricating the two-core or even four-core fiber optic intrinsically sensitive to the curvature Yuan et al. (2006, 2006). This scheme has been further used in the flow velocity sensor and accelerometer Yuan et al. (2006, 2008). They are all the applications of the homodyne demodulation. In addition, the fiber optic heterodyne interferometer has also been researched widely. Its measurement sensitivity can be improved because it can overcome the shortcomings of homodyne interferometer where the signal is easy to be influenced by the noises in the low frequency, such as the noises caused by the environment Liu et al. (2016); Wu et al. (2002).

The common mode noises (CMNs) suppression is used to reduce the background noises in Taiji program Liu and Luo (2021). Similarly, in fiber optic sensing field, the CMNs in interference optical layout include the periodic nonlinear noise caused by the laser beam, the imperfection of the beam splitters and the optical path noise of the other optical lens, etc. Wu et al. (2002). Some of these noises are shared by both the sensitive and the reference optical paths, the so-called CMNs. It is possible to reject CMNs by arranging the sensitive and reference optical paths in a symmetric design except for the sensing area Hechenblaikner (2013); Yi et al. (2018). Also, it is preferred to explore the extra optical path design with the gradually optimized CMNs suppression method Liu et al. (2016); Yi et al. (2018). However, almost all design schemes of interferometric sensor neglect the noises caused by the procedure of signal demodulation. As a result, the high accuracy CMNs suppression method referred in Taiji program is introduced to the fiber optic sensing field in this paper, although it has been used in the free-space optics before Hechenblaikner (2013).

To monitor the micro-deformation in Taiji program, we take an all-fiber-optic heterodyne interferometric sensor as an example, which is compatible with the configuration of the scientific interferometer, to prove the feasibility of the deformation readout when the fiber optic is pasted to the surface of the target components. This methodology allows not only the high precision deformation measurement by the introduction of the CMNs suppression, but also the contact deformation measurement without the generation of the stray light, which is very beneficial in Taiji program.

The Overall Arrangement of the Sensor

The complex and diverse deformation of the structure in the satellite is difficult to be described accurately. However, the structure can be simplified to be the one-dimensional or two-dimensional questions such as beams or plate sometimes. In that case, the fiber optic can be pasted on the surface of the target components. Here, as the pre-validation of methodology, the cantilever beam (CB) model is introduced to hold the fiber optics and the deformation of the CB can be read out by the fiber optic interference result.

Normally, the interference signal from sensitive interferometer is subtracted by the signal of reference interferometer to suppress the CMNs Liu et al. (2016). Analogous to the traditional CMNs suppression scheme, the optical path layout of the sensor proposed in this paper, which is sensitive to the environmental perturbation, is also based on the sensitive (CB1 as the main part) and reference (CB2 as the main part) interferometers with both the Michelson configuration, as indicated in Fig. 1. Each interferometer consists of both sensing beam and reference beam, which are displayed primarily by four reflective fiber optic, denoted by the red line. The environmental perturbation is represented by the black arrow at the end of CB1.

As shown in Fig. 1, the laser with a frequency of ω_0 is distributed via three fiber couplers (FC0, FC1 and FC2) to

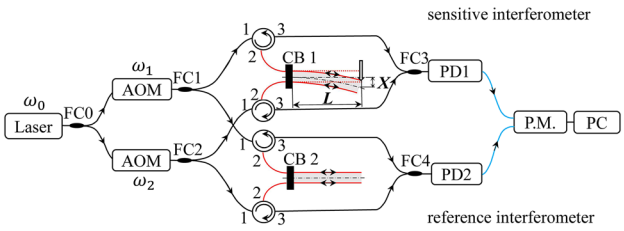

Fig. 1 Schematic diagram of the all-fiber-optic heterodyne interferometric sensor

the different interferometers. The heterodyne interferometry can be built up with two different angular frequencies, ω_1 and ω_2, by a pair of acousto-optic-modulators (AOMs), which can provide a frequency shift to the input signal. Four polarization-maintaining fiber optic circulators are essential to be introduced to realize the reflective optical path in the Michelson interferometer. Each circulator consists of three ports, by which the light signal can be transmitted in both assigned directions with low loss. The light signal entering the port 1 and then exiting from the port 2 is one of the directions, while the other direction represents the light entering the port 2 and leaving from the port 3. During this process, as the sensing elements, four reflective fiber optic play a significant role in the measurement of perturbation. This kind of reflective fiber optic is fabricated by coating with a reflective film with 90% reflectivity at the right end face of the fiber, while the other end can be connected to the circulators. These reflective fiber optics are stuck to the CB1 and CB2, where two parallel lengthwise grooves are prepared on the upper and lower surfaces. The black blocks located in the left end of the CBs in Fig. 1 indicate the fixed end of the CBs. After the circulators, four light beams are coupled in FC3 and FC4 and soon detected by the photodetectors PD1 and PD2, respectively, which transform the optical signal to the electrical signal. Subsequently, through the transmission lines marked in blue, the signals are input to the phasemeter (P.M.) to demodulate signals for the final interferometric phase fluctuation caused by the external perturbation. And the phase fluctuation measurement technology based on the digital phase locking loop (DPLL) is employed in our work Gerberding et al. (2013); Liu et al. (2018, 2021). Finally, the other relevant postprocessing analysis can be conducted on a followed personal computer (PC).

It can be observed in Fig. 1 that the designed optical path is highly symmetric for the purpose of suppressing the noises especially from photodetectors, transmission lines and phasemeter. This CMNs suppression scheme is similar to the one used in Taiji program. Besides, the CBs can not only fix the sensing reflective fiber optics, but also reflect the deformation of the sensing fiber optic when it is interfered by the external noise sources. As a result, the information of noise sources will be coupled into the optical path, and then can be read out through the final interference signals in a form of the change of OPD. The relation between the OPD ($\Delta\phi$) and the optical path noise (Δs) concerned is:

$$\frac{\Delta\phi}{2\pi} = \frac{\Delta s}{\lambda}, \tag{1}$$

where the λ is the optical wavelength of the laser.

To describe the micro-deformation quantitatively, we define the deflection X to be the variable perpendicular to CB, as shown in Fig. 1. And the final change of OPD can be expressed as the function of the change of deflection Yuan et al. (2006):

$$\Delta\phi = \frac{4k_0nd}{L}(1 - \frac{n^2}{2}c_2)\Delta X. \tag{2}$$

In this expression, k_0 is the wavenumber with the expression of $2\pi/\lambda$; n represents the refractive index of the fiber optic ($n = 1.458$); d is the width and height value of the CBs; L denotes the initial effective sensing length of the CB1 and $c_2 = 0.204$ is the constant related to the Pockels coefficients and the Poisson ratio of the fiber Peng et al. (2012); Yuan et al. (2006).

CMNs Modeling and Analysis

Except for the contact measurement with the fiber optic sensor, the high precision deformation measurement of the sensor is also the key technology worthy to be paid attention to. Hence, it is necessary to make the noise sources clear and then reduce the response impact on the optical path noise.

The general form of interferometric signals detected in the photodetector is expressed by the intensity:

$$I = Acos[2\pi(\omega_1 - \omega_2)t + \phi_0], \tag{3}$$

where A, ω_1, ω_2 and ϕ_0 denote the amplitude, the two angular frequencies after a pair of AOMs and the initial phase angle, respectively. Based on this expression, it is common practice to derive and analyze the suppression of the amplitude and phase noise Hechenblaikner (2013). But the lack of clarity still prevails about the CMNs sources and their corresponding effect mechanism. Here, the introduction and comparison are performed for the contributions of some important CMNs provided by the components in the proposed measurement chain.

The influence of the laser frequency noise due to the unequal arm-length interference can be neglected in our system Steier (2008). However, the noise from the AOMs should be taken into account. Based on the principle of diffraction, the functions of the AOMs are the frequency shift and the intensity modulation. The imperfect frequency shift signal

as well as the related signal actuation electronics both cause the optical frequency noise and yield to a phase fluctuation. Besides, the local thermal sources may be introduced from the AOM drivers and raise a higher requirement for the environmental thermal control.

In our all-fiber-optic sensor, it is worthy of noting that the fiber optic components are sensitive to the fluctuations of environmental thermal and vibration. Due to the system is located in the natural environment rather than a vacuum environment, the uneven environmental heat is distributed. Except for the heat conduction, the thermal convection also exits and results in the extra deformation of the fiber optic components. It will be coupled to the interference result according to the opto-elastic effect BoIler et al. (2009).

In addition, the all-fiber-optic sensor is distinguished from the other fiber optic sensor by rejecting the noises of the front-end electronics (FEE). The FEE contains the acceptance of the photocurrent through the photodetector, the translation of the photocurrent to the photovoltage, the digitization process of the Analog-to-Digital Converter (ADC) and a series of data processing of the digitized signals on the phasemeter Esteban Delgado (2012). During this process, some algorithmic noises should also be noticed, such as quantization noise during the digitization and the clock jitter noise. Generally, because the phase of the interferometric sensor is the main measurand aimed at, the FEE noises have been summarized in a form of the phase noises, mainly from the photodetectors, transmission lines and phasemeter separately. Specifically, the phase noise from the photo-detectors can be concluded as shot noise, electronic noise, thermal-induced phase noise and the finite phase response Barranco et al. (2018, 2017). The electrical signal is susceptible to the temperature fluctuation in the transmission lines. As regard to the phase noises of the phasemeter, the temperature coupling through finite phase response and flicker phase noise, caused by the electrical components, have been described in early studies Gerberding et al. (2015).

To sum up, the interference optical phase obtained in the sensitive interferometer and reference interferometer, with the same impact mechanism of the phase noise, can be given by Eqs. 4 and 5, respectively. ϕ_{AOM} denotes the phase noises caused by the AOM, whose impact is the same in both interferometers; In addition, ϕ_{FO}, ϕ_p, ϕ_t and $\phi_{P.M.}$ are the phase noises of the fiber optic components, photodetectors, transmission lines and phasemeter, respectively, in the sensitive interferometer. By contrast, ϕ'_{FO}, ϕ'_p, ϕ'_t and $\phi'_{P.M.}$ represent the related phase noises in the reference interferometer.

$$\phi_S = \phi_0 + \phi_{AOM} + \phi_{FO} + \phi_p + \phi_t + \phi_{P.M.} \tag{4}$$

$$\phi_R = \phi_0 + \phi_{AOM} + \phi'_{FO} + \phi'_p + \phi'_t + \phi'_{P.M.} \tag{5}$$

At last, the final interferometric signal can be derived by subtracting Eq. 5 from Eq. 4 to achieve the CMNs suppression, as shown in Eq. 6.

$$\phi = (\phi_{FO} - \phi'_{FO}) + (\phi_p - \phi'_p) + (\phi_t - \phi'_t) + (\phi_{P.M.} - \phi'_{P.M.}) \tag{6}$$

Comparing the phase results in Eqs. 4 and 6, the advantage of the CMNs suppression can be seen obviously. It is a common practice that the phase noise of the AOMs is rejected from the sensitive interferometer by introducing the reference interferometer. On the other hand, all other noises from the optical fiber components, photodetectors, transmission lines and phasemeter are suppressed to varying degrees through the subtraction process. Equation 6 is also instructive for building a sensor with better signal-to-noise ratio: as long as these components are close enough to each other to keep the external perturbations as small as possible, the unwanted phase noise from both the temperature variations and vibration can be reduced. All these points are meaningful for the design of the following experimental implementation.

Experiment

Experimental Setup

The performance of the contact all-fiber-optic sensor used for micro-deformation measurement is validated and the effect of the noise suppression is depicted experimentally in this section.

As shown in Fig. 2, the experimental setup of the optical system is established based on the schematic diagram of sensor mentioned in Fig. 1 and the noise suppression analysis in "CMNs Modeling and Analysis". The experiment was carried out at room temperature. Besides, it was tested in the nature environment, limited by the performance of the micrometer, which needs to be controlled manually.

The single-mode polarization maintaining laser with a wavelength of 1064 nm and power of 50 mW is used here for optical power stability of 1% and frequency stability of 1 MHz. The AOMs are aimed to modulate laser light to two continuous lights with the frequency of 130 MHz and 131.6 MHz respectively (generators driving the AOMs are not shown in the figure). The whole fiber optic included in the scheme are all polarization-maintained to avoid the noises caused by the polarized light. Besides, the circulators in the system are also polarization-maintaining fiber optic circulators (Thorlabs CIR1064PM-APC). The whole assembly of the fiber optic components before the sensing elements is firmly housed in the acrylic encloser 1 to keep them stable, since the fiber optic is sensitive to the environment perturbation. The free fiber fixing block is also set

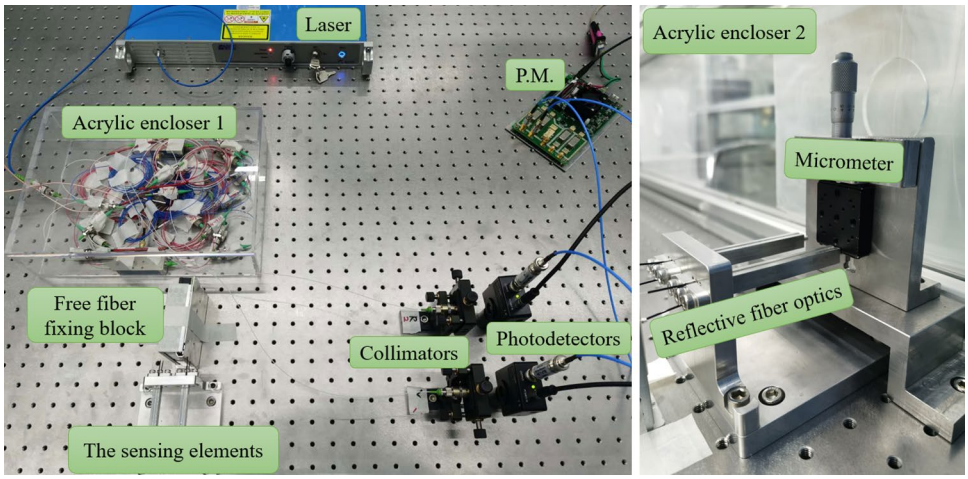

Fig. 2 The experimental setup of the optical system. Left: The experimental configuration of the system; Right: The detail view of the sensing elements

to keep the free fiber as stable as possible. After the fiber optic components, two optical fiber collimators are placed to improve the coupling efficiency. At the end of the system, the photodetectors used here are APD130C/M provided in Thorlabs. Afterwards, the signals received by the photodetectors are transmitted to the phasemeter through two transmission lines, which are the blue components as shown in Fig. 2. The basic parameters of the phasemeter such as the sampling frequency and the data output rate are 80 MHz and 60 Hz, respectively. The whole experimental system is wrapped in the acrylic encloser 2 to reduce the background noise of the system further. Unfortunately, the encloser 2 is big enough and its full view is not displayed in the figure.

The right part of Fig. 2 shows the configuration of the sensing elements. Two aluminium CBs have been chosen to fix the four reflective fiber optics as the sensing head. The cross-section sizes of the CBs are 8 mm*8 mm except for the two semi-circle gaps with the diameter of 1 mm located at the middle of the upper and lower surface of the two CBs. Here, the distance between the two reflective fiber optic is about 7 mm since the diameter of the fiber optic is nearly 0.05 mm. The fibers are cemented into their respective grooves by the adhesive NOA 61, which solidifies rapidly, deforms easily with the CB and is convenient to operate without premixes. At the free end of the CB, a cylinder with diameter and height of both 4 mm is machined for applying a known deformation (deflection X) perpendicular to the axis of the sensing CB by the micrometer, which provides a displacement increment of 0.01 mm.

Results and Discussion

It is important to measure the background noise of the sensor because the background noise determines the upper limit for the detection accuracy. The background noise can be obtained by long time data acquisition when the CB1 is not subject to any imposed deformation exerted by the micrometer. In our design of sensing scheme, the measured system background noise (phase fluctuation) based on a continuous piece of real-time data is shown in Fig. 3.

The data before suppression represent the interferometric results only from the sensitive interferometer, and the data after suppression are the subtraction results between the sensitive and reference interferometric signals. The result shows that the phase fluctuation of the background noise has been reduced. Specifically, the standard deviation of the phase fluctuation after suppression can reach 0.03756 rad, while the value before suppression is 0.5233 rad. The reduction of the phase fluctuation benefits from the elimination of the CMNs, including the environmental and electronics noises, and it shows the probability to improve the measurement accuracy for the sensor.

To validate the sensing performance of the sensor, five groups of experiments have been carried on, where the CB1 is subject to the specific imposed deformation exerted by the micrometer. During the experiment, the efficient length L of the sensing beam is chosen to be 90 mm. In each group of experiments, a displacement increment of 0.01 mm is forced to the CB1 every few seconds, a total of five times. As a result, the change of OPD ($\Delta\phi$) corresponding to the change of deflection (ΔX) for each step is recorded. In terms of the obtained data of five repeat experiments (before or after suppression), the characteristics of the sensor can be described and the comparison of theoretical prediction and experimental results is given in Fig. 4.

First, the slopes of both experimental fitting curves are different with that of the theoretical curve. To be specific, the measurement error between the theoretical formula and the interference result after the CMNs suppression is found to be 3.5 %, which is eight times smaller than the error of the experimental results before suppression. It should be noted that the linear coefficient of the first order fitting curve is the average value of the five repeated experiments. Thus, the performance of the CMNs suppression has been certified effectively.

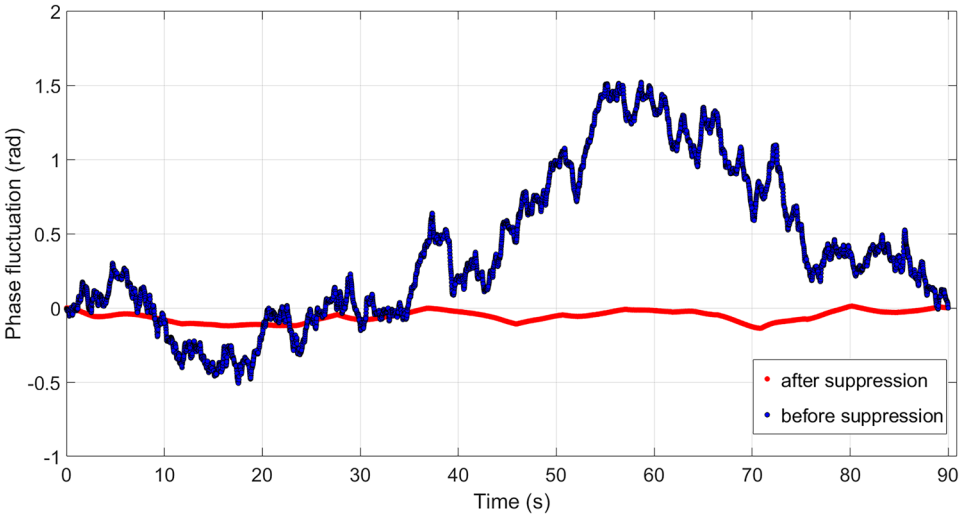

Fig. 3 The background noise of the sensor

Besides, it can be seen from Fig. 4 that the linear coefficient of the experimental fitting curve after the CMNs suppression is 2.178×10^6 rad/m. However, the theoretical prediction is calculated as 2.104×10^6 rad/m from Eq. 2. The mismatch error can be partly explained as follows: The theoretical result is just an approximation guide to the experimental result considering that the parameters used in the theoretical analysis are chosen by experience, such as the refractive index of the fiber optic. On the other side, the environment noise including both the vibration and the thermal perturbation may not be completely negligible. Moreover, the influence of the adhesive bonding technology also needs to be considered further.

Furthermore, the error bars of the five experimental results are provided. The experimental fitting curves are both almost within the range of the error bar, which means that the fitting curves obtained are effective in the repeated experiments.

In brief, the linear relationship of the sensing scheme after suppression adequately aligns with the theoretical predictions with the acceptable tolerance for error. It means the sensing relationship between the change of OPD ($\Delta\phi$) and the change of deflection (ΔX) of the sensor proposed in this paper is

$$\Delta\phi = 2.178 \times 10^6 \Delta X. \tag{7}$$

It proves the feasibility of the contact micro-deformation measurement by the all-fiber-optic interferometric sensor. In addition, the measurement error of the change of deflection in this sensor is reduced from 240 nm to 17.2 nm through the optimized CMNs suppression scheme, which reflects a good noise suppression performance.

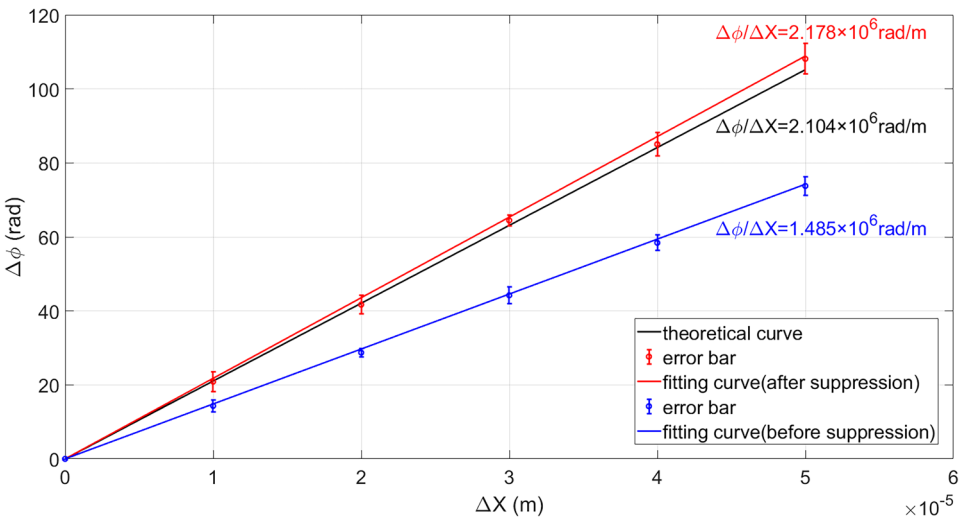

Fig. 4 Comparison of the theoretical prediction and experimental results of the sensor

Conclusions

Taking the cantilever beam, on which the fiber optic is pasted, as an example, it proves that the all-fiber-optic interferometric sensor can be applied to the micro-deformation measurement. On the one hand, the experimental results show that the linear relationship of the sensing scheme adequately aligns with the theoretical predictions with the acceptable tolerance for error. It proves the feasibility of the contact micro-deformation measurement by the all-fiber-optic interference sensor without the generation of the stray light. On the other hand, the measurement error of the change of deflection in this sensor is reduced from 240 nm to 17.2 nm through the CMNs suppression, which shows the realization of the high precision deformation measurement. With the pre-verification of this methodology, it provides a new choice for future Taiji program to monitor the deformation of the internal structures with no need to build the spatial optical path, followed by reducing its influence on the optical path noises to reach the final requirement of Taiji program.

Acknowledgements This work was supported by the National Key R&D Program of China (Grant No. 2020YFC2200104) and the Strategic Priority Research Program of the Chinese Academy of Sciences (Grant No. XDA1502110102).

Data Availability The data that support the findings of this study are available from the corresponding author upon reasonable request.

Declarations

Conflict of Interest The authors declare no conflicts of interest.

References

Barranco, G.F., Gerberding, O., Schwarze, T.S., Sheard, B.S., Heinzel, G., Dahl, C., Zender, B., Heinzel, G.: Phase stability of photoreceivers in intersatellite laser interferometers. Opt. Express **25**, 7999–8010 (2017)

Barranco, G.F., Sheard, B.S., Dahl, C., Mathis, W., Heinzel, G.: A low-power, low-noise 37-MHz photoreceiver for intersatellite laser interferometers using discrete heterojunction bipolar transistors. IEEE Sens. J. **18**, 7414 (2018)

Boller, C., Chang, F.K., Fujino, Y.: Encyclopedia of structural health monitoring. John Wiley & Sons, Ltd (2009)

Butter, C.D., Hocker, G.B.: Fiber optics strain gauge. Appl. Opt. **17**, 2867–2869 (1978)

Esteban Delgado, J.J.: Laser ranging and data communication for the laser interferomter space antenna, Ph.D. thesis (Gottfried Wilhelm Leibniz Universität Hannover, 2012)

Gerberding, O., Diekmann, C., Kullmann, J., Tröbs, M., Bykov, I., Barke, S., Brause, N.C., Delgado, J.J.E., Schwarze, T.S., Reiche, J., Danzmann, K., Rasmussen, T., Hansen, T.V., Enggaard, A., Pedersen, S.M., Jennrich, O., Suess, M., Sodnik, Z., Heinzel, G.: Readout for intersatellite laser interferometry: Measuring low frequency phase fluctuations of high-frequency signals with microradian precision. Rev. Sci. Instrum. **86**, 074501 (2015)

Gerberding, O., Sheard, B., Bykov, I., Kullmann, J., Delgado, J.J.E., Danzmann, K., Heinzel, G.: Phasemeter core for intersatellite laser heterodyne interferometry: modelling, simulations and experiments. Class. Quantum Gravity **30**, 235029 (2013)

Hechenblaikner, G.: Common mode noise rejection properties of amplitude and phase noise in a heterodyne interferometer. J. Opt. Soc. Am. **30**, 941–947 (2013)

Hu, W.R., Wu, Y.L.: The Taiji Program in Space for gravitational wave physics and the nature of gravity. Natl. Sci. Rev. **4**, 685 (2017)

Hu, W.R., Kang, Q.: Frontiers of microgravity science. Sci. Tech. Rev. **38**, 59–62 (2020)

Liu, H.S., Luo, Z.R.: In-orbit performance of the laser interferometer of Taiji-1 experimental satellite. Int. J. Mod. Phys. A **36**, 2140004 (2021)

Liu, H.S., Luo, Z.R., Jin, G.: The Development of Phasemeter for Taiji Space Gravitational Wave Detection. Microgravity Sci. Technol. **30**, 775 (2018)

Liu, H.S., Yu, T., Luo, Z.R.: A low-noise analog frontend design for the Taiji phasemeter prototype. Rev. Sci. Instrum. **92**, 054501 (2021)

Liu, F., Xie, S.R., Qiu, X.K., Wang, X.F., Cao, S., Qin, M.Z., He, X.G., Xie, B., Zheng, X.P., Zhang, M.: Efficient common-mode noise suppression for fiber-optic interferometric sensor using heterodyne demodulation. J. Lightwave Technol. **34**, 5453–5461 (2016)

Luo, Z.R., et al.: The recent development of interferometer prototype for Chinese gravitational wave detection pathfinder mission. Opt. Laser Technol. **105**, 146 (2018)

Malki, A., Lecoy, P., Marty, J., Renouf, C., Ferdinand, P.: Optical fiber accelerometer based on a silicon micromachined cantilever. Appl. Opt. **34**, 8014–8 (1995)

Peng, F., Yang, J., Wu, B., Yuan, Y.G., Li, X.L., Zhou, A., Yuan, L.B.: Compact fiber optic accelerometer. Chin. Opt. Lett. **10**, 011201 (2012)

Sun, S.Y., Liu, Y., Mohamed, A.: Sharaf Eldean, Design and implementation of an optical fiber sensing based vibration monitoring system. J Vibroengineering **23**, 496 (2021)

Sun, J.X., Yang, J., Liu, Z.H., Yuan, L.B.: Laser interferometer used for nanometer vibration measurements. Proc. SPIE **6595** (2007)

Steier, F.: Interferometry techniques for spaceborne gravitational wave detectors, Ph.D. thesis (Gottfried Wilhelm Leibniz Universität Hannover, 2008)

Tröbs, M., d'Arcio, L., Barke, S., et al.: Testing the LISA optical bench (2013)

Vallée, R., Drolet, D.: Practical coupling device based on a two-core optical fiber. Appl. Opt. **33**, 5602–5610 (1994)

Wang, A., Miller, M.S., Plante, A.J., Gunther, M.F., Murphy, K.A., Claus, R.O.: Split-spectrum intensity-based optical fiber sensors for measurement of microdisplacement, strain, and pressure. Appl. Opt. **35**, 2595–601 (1996)

Wu, C.M., Lin, S.T., Fu, J.: Heterodyne interferometer with two spatial-separated polarization beams for nanometrology. Opt. Quant. Electron. **34**, 1267–1276 (2002)

Yuan, L.B., Yang, J., Liu, Z.H., Sun, J.X.: In-fiber integrated Michelson interferometer. Opt. Lett. **31**, 2692–2694 (2006)

Yuan, L.B., Liu, Z.H., Yang, J.: Coupling characteristics between single-core fiber and multicore fiber. Opt. Lett. **31**, 3237–3239 (2006)

Yuan, L.B., Yang, J., Liu, Z.H.: A compact fiber-optic flow velocity sensor based on a twin-core fiber Michelson interferometer. Sensors Journal, IEEE **8**, 1114–1117 (2008)

Yi, D., He, X.G., Liu, F., Gu, L.J., Zhang, M., Qiu, X.K., Ye, H.: Self-suppression of common-mode noises of the different fiber optic interferometric accelerometers. Opt. Express **26**, 15384–15397 (2018)